

Dual-Energy Computer Tomography and Digital Radiography Investigation of Organic and Inorganic Materials

Mihai IOVEA, Marian NEAGU, Accent Pro 2000, Ltd, Bucharest, Romania
Octavian G. DULIU, University of Bucharest, Department of Atomic and Nuclear Physics,
Bucharest, Romania

Gheorghe OAIE, National Institute of Marine Geology and Geoecology, Bucharest,
Romania

Calin RICMAN, Geological Survey of Romania, Bucharest, Romania
Gabriela MATEIASI, The Politehnica University, Bucharest, Romania

Abstract. By means of a home made X-ray dual-energy computer tomography (CT) provided with a double set of X-ray detector arrays separated by a copper foil and by using a proper variant of filtered back projections reconstruction algorithm together with a set of well calibrated standard samples we have been able to determine with a precision varying between 3.5 % and 2 % the density as well as the effective atomic number distribution in any section of a great diversity of samples.

In this way it was possible to discriminate different domestic materials that on a normal radiography generate the same signature such as soap, paper, leather, tooth past, the content of spray tubes, etc.

The same CT has been use to investigate different geologic samples consisting of sediment cores collected at depth up to 600 m from the continental platform of the Black Sea and fragments of metamorphic rocks collected from the Sibischel shear zone from the Central Carpathian mountains. In the case of deep sea cores we have evidenced about 225 distinct laminae, 2 to 4 mm thick that by means of time series analysis revealed a periodicity of about 7 years, while in the case of metamorphic rocks we have observed diverse features such as garnet size and distribution, shear zones, mica laminations, etc. Numerical values of both density and especially effective atomic numbers allowed distinguishing between natural silicates and calcium carbonates, irrespective of the host rock.

1. Introduction

Computer axial tomography (CAT) represents a non-destructive method of investigation which, since its first application three decades ago as a medical examination technique [1], now has become a routine procedure with numerous applications in various fields such as industry [2-5], geosciences [6-10], physics [11,12], life sciences [13-16], etc. Based on the attenuation of high energy gamma or X ray or in some instances neutrons [17,18], CAT generates digital images which illustrate the distribution function of the linear attenuation coefficient (LAC) within a planar section [19-21] or an entire volume [22-25] of the investigated object.

The essence of this method consist of reconstructing the distribution function of the LAC within a chosen section (planar or volumic) by starting from a set of numerical values of the projections of this parameter taken all around the investigated sections (Figure 1).

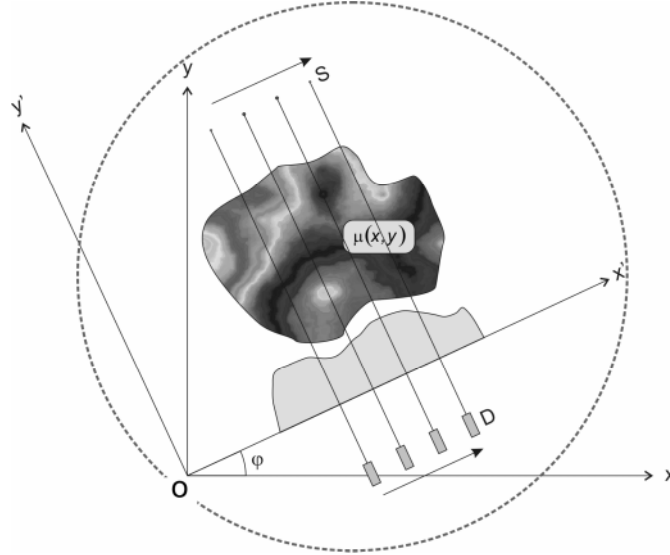


Figure 1 LAC projection acquisition in a plan-parallel geometry is realized by successive displacements of both radiation source (S) and detector (D) on a direction OxD' perpendicular to $OyD'X'$ - or gamma ray direction. Successive positions of source-detector system allow the acquisition of LAC linear projection defined as the transmittance logarithm. Dashed circle represents the reconstruction space. For a better illustration the origin of both systems of references were represented far from the object, while, in reality they are placed in the section center.

The main advantage of using high energy nuclear radiation consists of the acquisition of the LAC projections by measuring the current density I of transmitted X- or gamma ray quanta for consecutive positions along a direction perpendicular to the incident radiation, according to the equation:

$$\begin{aligned} \lambda_{\varphi}(x') &\equiv -\int_s^D \mu(x, y) dy' = -\ln \frac{I}{I_0} = \\ &= \int_{-\infty}^{+\infty} \int_{-\infty}^{+\infty} \mu[x, y] \delta(x \cos \varphi + y \sin \varphi - x') dx dy \end{aligned} \quad (1)$$

where: $\lambda_{\varphi}(x')$ represents the numerical value of LAC projection along the direction xD' , $\mu(x, y)$ is the LAC distribution function in the chosen section, I_0 is the current density of incident radiation.

Reconstruction of the LAC distribution over investigated section is best performed by means of filtered back projection method [19, 26] although other methods such as iterative least squares technique [27] or the algebraic reconstruction [28] gave good results.

To reduce the acquisition time, almost all computer tomographs (CT) are provided with high output X-ray tubes, working at an anodic potential up to 200kV at a current up to 100 mA. In this way, a CAT image can be obtain in less than 1 s, this fact making CAT one of the fastest method of non-destructive control.

On the other hand, the use of X-ray tubes that generate a polychromatic radiation whose energy varies between 30 and hundreds of keV, generate some undesirable artifacts on the reconstructed tomographies. The most significant of them, the beam hardening, needs mathematical [20, 28] or physical correction [29].

It is worth to mention that the LAC of any material or element represents the product between density ρ and the mass attenuation coefficient (MAC), the last one depending only on effective atomic number and X- or gamma ray energy, according to the relation [30]:

$$\mu(E, Z) = \rho \left[a(E) Z_{eff}^{c(E)} + b(E) Z_{eff} \right] \frac{\mathcal{N}_A}{A_{eff}} \times 10^{-24} \quad (2)$$

where Z_{eff} is the effective atomic number; \mathcal{N}_A is the Avogadro's number; A_{eff} is the effective mass number; $a(E)$, $b(E)$ and $c(E)$ are some numerical coefficients whose values that depend only on the energy of X- or gamma ray are usually determined by using a number of standard samples [30].

In Eq. (2), the first term describes the photoelectric effect, important for energies below 100 keV and low atomic numbers while the second term accounts for Compton inelastic scattering that is predominant for energies higher than 100–200 keV. In the case of heavier elements such as iron, copper or lead, the LAC depends less or more on the atomic number even for higher than 200 keV energies [31].

Consequently, for mineral samples containing both low and high atomic number elements, the only quantitative information that can be inferred by analyzing CAT images mainly referees to the local valued of LAC, which, in some cases could be insufficient for a more detailed analysis.

This inconveniency was significantly overcome by using a dual-energy CAT (DECAT) [30,32–36] that, by measuring the same section through investigated sample by means of two X- or gamma rays having different energies it makes possible the determination of both density and effective atomic numbers distribution functions through chosen section.

Although radioisotopic monochromatic gamma-rays sources such as ^{169}Yb (50.4 keV), ^{241}Am (59 keV), ^{192}Ir (310.5 and 469.1 keV) or ^{137}Cs (662.7 keV) gave the best results, almost similar DECAT images were obtained by means of polychromatic X-rays provided that the transmitted radiations are detected by means of sets of two different detectors separated by a thin (1 to 2 mm) copper shield. Due to its high density, this metallic foil acts as a filter for the low energy X-rays, which considerably modifies the spectral composition of the radiation detected by each set of detectors. Coupled with an appropriate collection of standard samples with well known densities and atomic numbers, and by using suitable reconstruction algorithms, two different CAT images of the same sections are finally computed. One of them depicts the densities, while the other one represents the Z_{eff} distribution over the investigated sections. Depending on the chosen standards, the error for density determination can reach 3.5 % while the corresponding error for Z_{eff} was no greater than 3% [present paper, 37].

In this way, DECAT is able to discriminate two materials having the same density and different effective atomic number such as plastic explosives and soap, chocolate or other similar goods currently existing in luggage [Lovea et al., present paper] or different minerals such as quartz or calcite [35–37].

Besides reconstructing images from projections, any CT provided with a linear set of detectors, can be successfully used to obtain high resolution digital radiographs by translating the object between X-ray tube and detectors. This variant of digital radiography (DR), firstly presented in ref. [38] to investigate sedimentary cores provides high resolution images completely free of parallax error as the field of view is usually thinner than 1 mm. It must be pointed out that especially in the case of sedimentary cores DR shown to be very suitable, as, due to their perfect cylindrical shape, the most information concerning the distribution as well as the reciprocal orientation of different layers that compose this kind of core could be very well evidenced and eventually investigated by analyzing corresponding DR images [39].

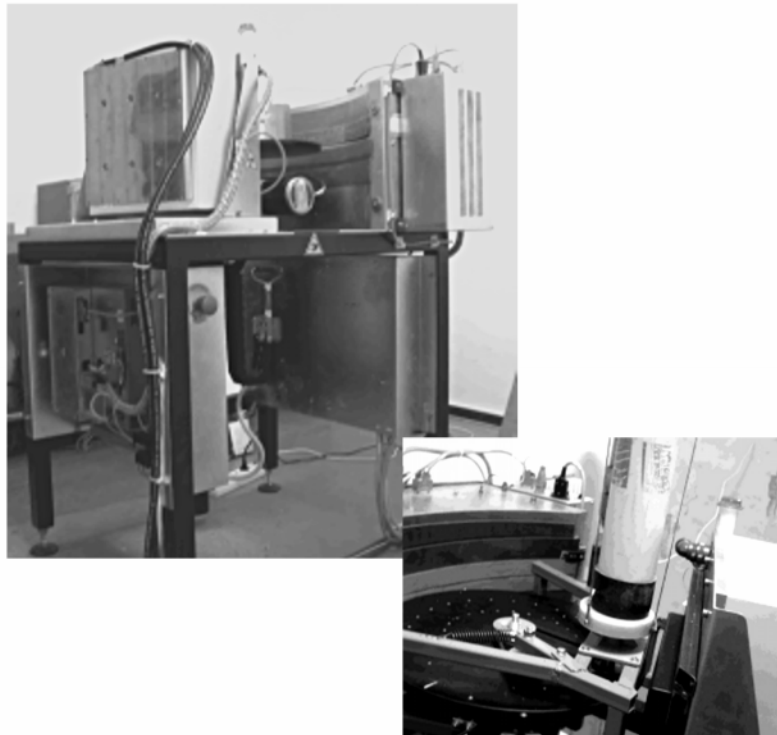


Figure 2 A general picture of the dual-energy CT used for this study. The inset depicts the small diameter table with o core fixed for investigation.

In this paper we present the most important results obtained in investigating, by means of DECAT and DR, different domestic materials as well as various geological samples from the collection of National Museum of Geology and National Institute of Marine Geology and Geoecology, Bucharest.

2. Materials and Methods

2.1 Dual-energy CT

All measurements have been performed by using a home-made dual energy CT (DECT) designed and built in co-operation by *Accent Pro 2000 Ltd* (www.accent.ro) and *Gilardoni S.p.A.* (www.gilardoni.it) companies (Figure 2). The DECT was provided with 160 keV/3mA X-Ray source and a number of 980 photodiode with scintillator as radiation detectors mounted in a dual-energy radial arrangement (Figure 2). In order to perform DECAT investigation of different diameter sample, the DECT has two rotating tables, one of 40 and the other 10 cm diameter. Accordingly, the spatial resolution varied between 0.8 and 0.3 mm respectively. In both configurations, the total scanning time was about 16 seconds for 241 projections and the corresponding reconstruction time for a 400x400 pixels DECAT image was about 7 seconds. The LAC reconstruction was performed by a filtered back projection algorithm [39].

The same DECT was used to obtain digital free-of-distortion radiographs by moving the objects vertically normally crossing the X-Ray fan beam, with a speed of about 10 cm/minute. In the case of any interesting features observed during scanning, the vertical shift has been stopped allowing to obtain DECAT images of any desired sections.

Table 1 Numerical values of low and high energy LAC (in cm^{-1}), densities and Z_{eff} numbers: physical and calculated by means of eq. (2)

Material	μ_l	μ_h	ρ	ρ_{DECAT}	$\varepsilon(\rho)$	Z_{eff}	Z_{eff}^{DECAT}	$\varepsilon(Z_{eff})$ %
Polyamide 12	0.0926	0.0813	1.016	0.9959	-1.974	6.1579	6.0963	-1.288
Polyetherimide	0.1121	0.0968	1.274	1.2375	-2.863	6.4000	6.3989	-0.017
Polyoxymethylene	0.1415	0.1180	1.493	1.5452	3.494	7.1204	7.2534	1.868
Graphite	0.1519	0.1325	1.797	1.8366	2.206	6.000	5.9276	-1.206
Teflon	0.1970	0.1580	2.171	2.1256	-2.101	8.4689	8.4570	-0.140
Polyphenylenesulphide	0.2113	0.1436	1.620	1.6303	0.637	11.1708	11.4671	-0.034

The numerical values of the LAC corresponding to the two sets of detectors has been transformed into densities and Z_{eff} values by means of experimental calibration curves obtained by using minimum six different standard materials with known densities and effective atomic numbers (Figure 3). For a better interpretation of the DECAT pictures, for each density as well as Z_{eff} images, the corresponding histograms were calculated [36].

2.2 Samples

We have investigated three main categories of samples, *i.e.* organic materials having densities and consistencies close to plastic explosives, fragments of metamorphic rocks (linear mica-rich gneisses, a garnet bearing micaschist and a layered mylonite), collected from the Sibischel shear zone from the Central Carpathian mountains (Sadu and Cugir valleys) and a standard core consisting of five layers of calibrated sand together with three sets of 4 unconsolidated sediments core collected downstream the confluence of the Danube River with the Danube-Black Sea Channel (near Cernavoda municipality), from the Danube Delta (Sulina Channel mouth) as well from the Continental Platform of the Black Sea depth varying between 40 m and 600 m. For calibration, we have used a standard core composed of five layers of calibrated quartz sand with a small amount of clay. Our intention in analyzing such different samples was to demonstrate the large possibilities of investigation our instrument or other similar ones have.

3. Results and discussion

3.1 Organic materials

For this study we have chosen six different organic materials (polyamide 12, polyetherimide, polyoxymethylene, graphite, teflon and polyphenylenesulphide, produced by Ensinger GmbH, Nufringen, Germany) with calibrated densities and effective atomic numbers (Table 1). The numerical values of density as well as Z_{eff} have been obtained by a best fit method starting from the experimental DECAT data.

In this way, starting from the experimental numerical values of LAC corresponding to low (front) end high (rear) energy detectors, it was possible to calculate both density and Z_{eff} numerical value of investigated materials. The values thus calculated differed by the real ones with maximum 3.5 % for densities and less than 2% for Z_{eff} (Table 1).

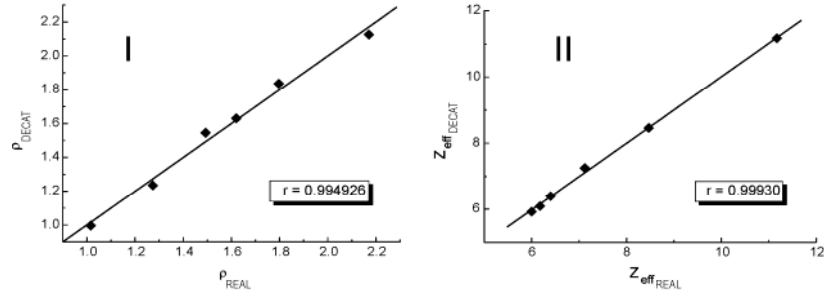


Figure 3 Density (I) and effective atomic number (II) calibration curves experimentally obtained by using different materials with known densities as well as chemical compositions (polyamide 12, polyetherimide, polyoxymethylene, graphite, teflon and polyphenylenesulphide).

At the same time, the correlation coefficient between physical and DECAT calculated values of these parameters was equal to 0.994956 for densities and 0.99930 for Z_{eff} which means a significant correlations with $p < 0.05$ (Figure 3).

In these conditions we have been able to discriminate different domestic materials that on a normal radiography generate the same signature such as chocolate, soap, paper, leather, tooth past, the content of spray tubes, etc.

3.2 Metamorphic rocks

In Figure 4 are reproduced the most representative DECAT images of investigated rocks by means of low energy LAC, density and effective atomic number, while Table 2 contains numerical data concerning the last two parameters.

In the case of linear mica-rich gneiss, LAC image reveals the presence of two different components, while the layered structure, typical for the gneiss is relatively well illustrated on both Z_{eff} and density pictures.

On the lower part of the LAC image it can be observed a singular eye-shaped garnet with different density and mineralogical composition. On density and Z_{eff} images the presence of hidden planes, the shear band geometry, the tails in pressure shadows formed in the softening reaction of rigid grains in the mylonitization process and also by dynamic recrystallization could be observed too.

Table 2 Numerical values of density and Z_{eff} of investigated metamorphic rocks as determined by analyzing images histograms, together with the numerical values of the same parameters for the most common constituents of investigated samples

Rock	ρ (g/cm ³)	Z_{eff}	Mineral	ρ (g/cm ³)	Z_{eff}
linear mica-rich gneiss	1.6 – 3.6	10.8 – 13.9	albite	2.48	11.3
			quartz	2.51	11.4
garnet bearing micaschist	3.5 – 4.5	7.1 – 14.5	anorthite	2.70	12.8
			muscovite	3.25	13.2
layered mylonites	2.7 – 4.4	8.8 – 12.5	grossular	3.82	14.5

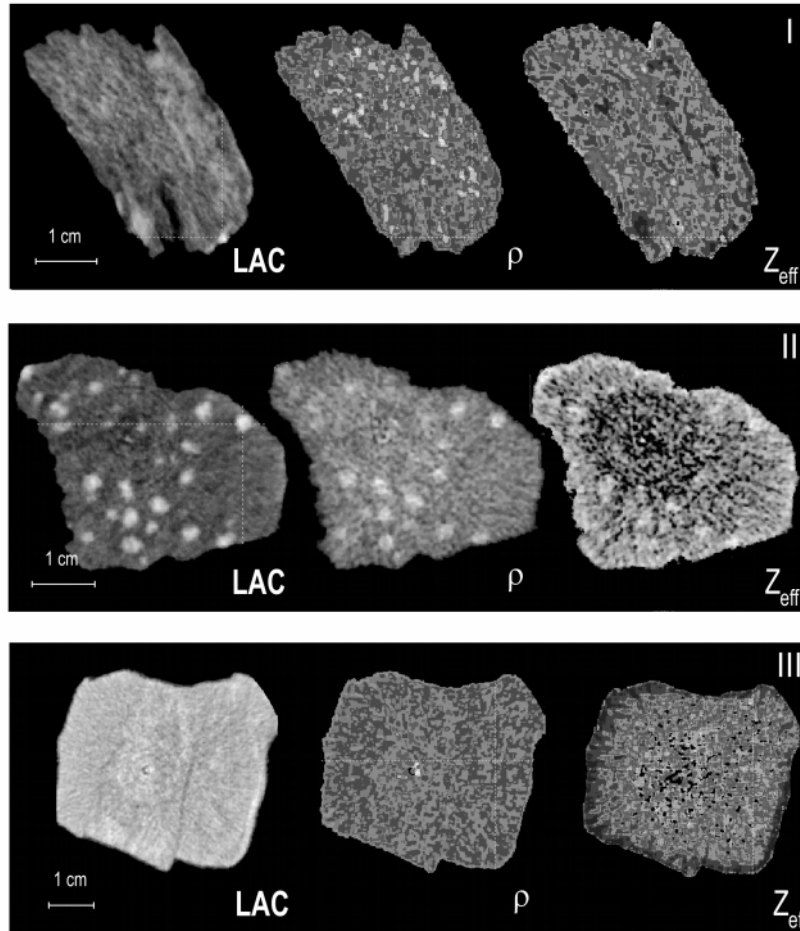


Figure 4 DECAT images of linear mica-rich gneisses (I), a garnet bearing micaschist (II) and a layered mylonite (III). For each sample the low energy LAC (μ), densities (ρ) as well as Z_{eff} distributions are reproduced.

Concerning the garnet bearing micaschist, both low-energy LAC and density CAT images show a number of well developed garnets whose slightly ellipsoidal shape attests the existence of subsequent movements to whom the formation of the present foliation could be attributed. It must be pointed out that on Z_{eff} images the garnets are almost undistinguishable, this fact pleading for a close chemical composition of garnets and surrounding matrix.

The most probable, the garnet crystallization growth has been very rapid in the first growth interval (the central zone being generally rich in inclusions) and slows in the final growth period, when the clear marginal zone was formed.

For the last sample, the layered mylonites, both LAC and densities DECAT images clearly reveal two fractions, a very fine chlorituous one, and a biotitic quartzose coarser one, with a lower density. A cataclastic flow can be observed looking at the areas with different textures. Otherwise, the sample seems to be relatively homogenous by respect to densities but more inhomogeneous from the point of view of the chemical composition as Z_{eff} image suggests.

As it results from the Table 2, there is a good concordance between the numerical values of density and Z_{eff} of investigated metamorphic rocks as determined by analyzing images histograms and the corresponding values of the same parameters of the major component minerals.

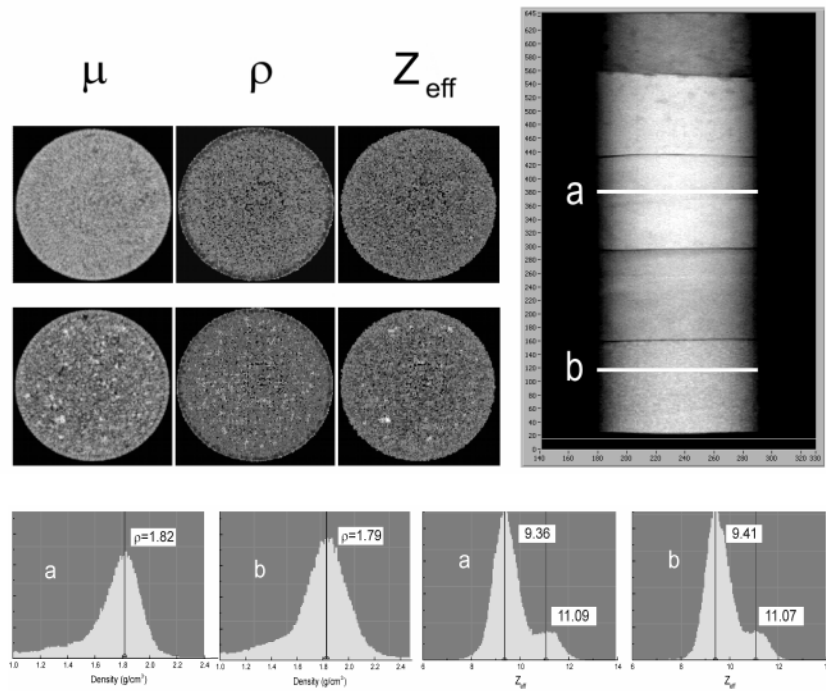


Figure 5 Six DECAT images (upper, left) illustrating the low energy tomographies (μ), densities (ρ) as well as Z_{eff} distributions corresponding to sections *a* and *b* of DR image of a standard core (upper right) while the lower images represents both densities and Z_{eff} histograms of sections corresponding sections.

3.3 Unconsolidated sediments

Since cores, as previously has been stated, represent object with an almost perfect cylindrical shape, in many cases and especially in the case of fine laminated sediments the most important features were observed on DR images. To illustrate this peculiarity in Figure 5 we have reproduced a DR of the standard core together with six different DECAT images corresponding to two different transverse sections that reproduce the distribution of low-energy LAC (μ), density ρ as well as Z_{eff} . It must be pointed out the resemblance between LAC and density CT images, explained by an almost identical chemical composition of investigated sections, mainly consisting of quartz with small amount of clay. At the same time, the sand granularity is better illustrated on the lower section, because in this case, the average grain sizes are significantly greater than the maximum spatial resolution, estimated to 0.5 mm. A more detailed analysis performed by means of

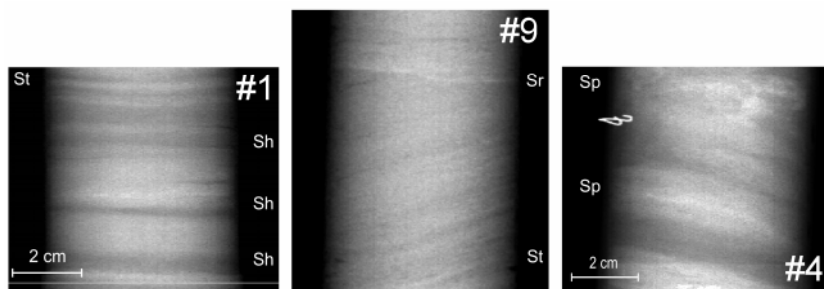


Figure 6 Three most representative DR images of cores collected from the Danube River bed, near Cernavoda. Different lithofacieses such as horizontally bedded sand (Sh), ripple cross laminations in medium to very fine sand (Sr), trough cross bedded sediments (St) or planar cross bedded sand (Sp) could be observed on these images.

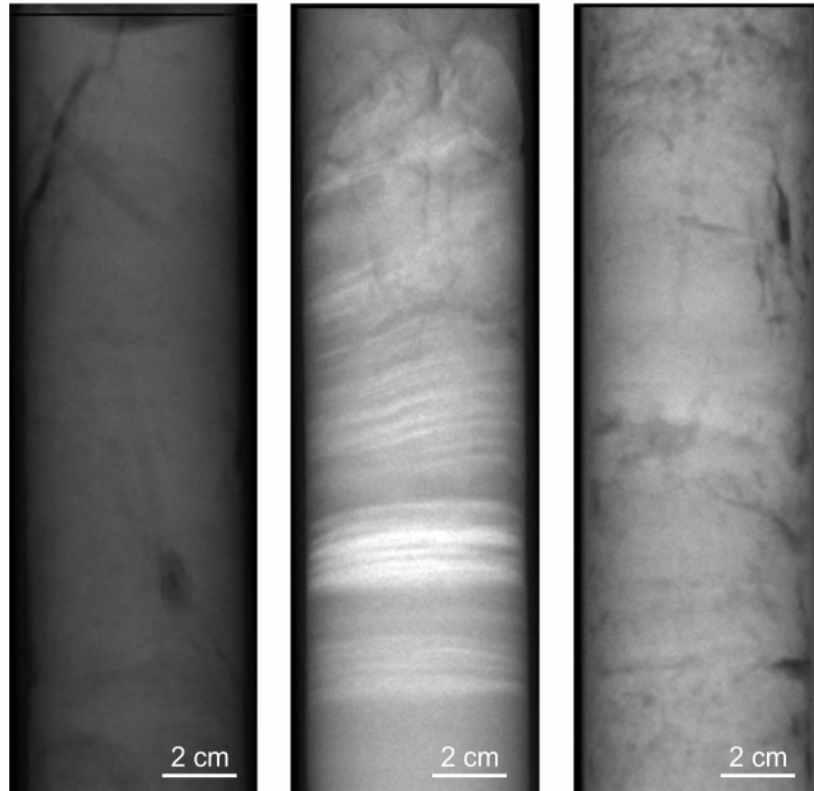


Figure 7 DR of the upper part of three cores collected from the Danube Delta (Sulina Channel mouth) showing a great variety of lithofacieses. The planar cross bedded laminae observed on the inferior part of the middle core represents highly mineralized sediments containing a considerable amount of heavy minerals such as rutile and zircon. The dark colour of the first core is due to a considerably amount of unconsolidated mud while the third core is relatively rich in vegetal debris.

tomographies histograms (Figure 5) has shown that in both cases, the sand density was almost the same, i.e. between 1.79 and 1.82 g/cm^3 while Z_{eff} histograms clearly revealed the presence of two different fractions, a dominant lighter one corresponding to quartz and a heavier one, less abundant, most probably due to the presence of small amount of clay. It is worth to mention that, as Z_{eff} histograms show, in both cases, the chemical composition, irrespective of grain sizes, was very similar.

For all other cores, due to a relative homogeneity within any investigated sections, the most information was obtained by analyzing corresponding DR images, results which will be discussed below.

As regards Danube River cores (Figure 6), all DR images illustrate different lithofacies types characteristic for a river bed [40], such as trough cross bedded sediments (St), made by sand as tabular sets; ripple cross laminations in medium to very fine sand (Sr), with an irregular base, the foreset position indicating the water current direction; planar cross bedded sand (Sp), formed by dunes migration when very fine to medium sand is transported by traction or in suspension with redeposition as foreset laminae; horizontally bedded sand (Sh) showing a parallel lamination, the structure being stable for very fine to medium sandy sediments.

Danube Delta sediments (Figure 7) shown to be more diverse, a typical particularity for a zone characterized by a great variety of physico-chemical conditions due to the interaction with a variable salinity sea water as well as to a more complicate local circulation, both this factors contributing to a differential deposition of minerals that compose the sediments.

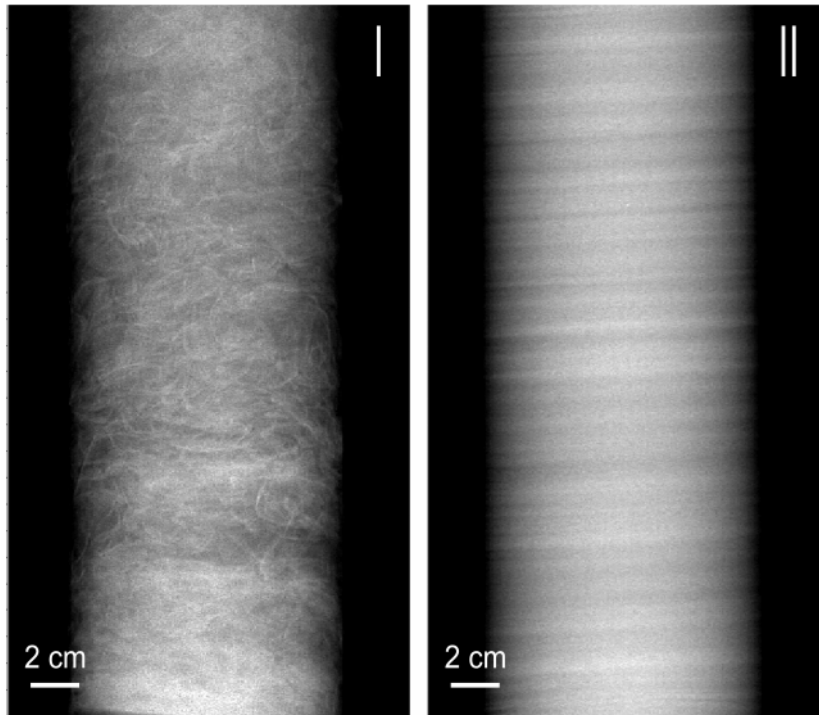


Figure 8 DR images of two Black Sea bottom cores collected at a depth of 40 mm (I) and of 600 m (II). The left core consist of an alternation of horizontal bedded sand and mussel debris agglomeration, typical for a mussel-rich facies characteristics for this depth. The right one is composed by almost horizontal fine laminae, without any trace of bioturbation, specific for the anoxic zone of the Black Sea. The slightly inclinations of some groups of laminae could be attributed to a very slow bottom current.

As a result we have been able to identify a depositions zone with an appreciable concentration of heavy minerals such as rutile and zircon, whose presence can be immediately remarked on DR like a group of significantly more opaque laminae (Figure 7).

On contrary, the Black Sea core presents two completely different structures reflecting the depth they were collected. Specific to the Black Sea is the presence of an abiotic zone, contaminated by hydrogen sulfide, and populated only by adapted bacteria. This zone that exists below a depth of about 70 to 100 meters at the center and 110 to 150 meters near the edge and whose sediments are free of any trace of bioturbation is very promising by taking into account the presence of almost unaltered laminae that practically retain significant intervals of geological history of the Black Sea.

Accordingly, we have investigated two different types of cores, one collected above the hydrogen sulfide layer and consisting mainly of a mixture of silt and fragments of *Mytilus galloprovincialis* Lamarck mussels and the other one, within the hydrogen sulfide water consisting of a fine alternation of almost unperturbed varves (Figure 8).

In the first case, both DR and CAT images has shown the presence of a considerable amount of mussel shells, in alternation with horizontal bedded sands, what confirm the presence at these depth of the typical mussel-rich facies, a characteristic of the Black Sea low depth bottom, [41]. More interesting appeared the core collected at 600 m below sea level, in the anoxic sector of the Black Sea. According to images reproduced in Figure 8, the structure of these sediments consists of an alternation of almost horizontal, fine laminae without any trace of bioturbation. This fact appears more interesting as at carefully examination of the core, visible through the transparent wall of the corer, no sign of any fine laminated structures were observed.

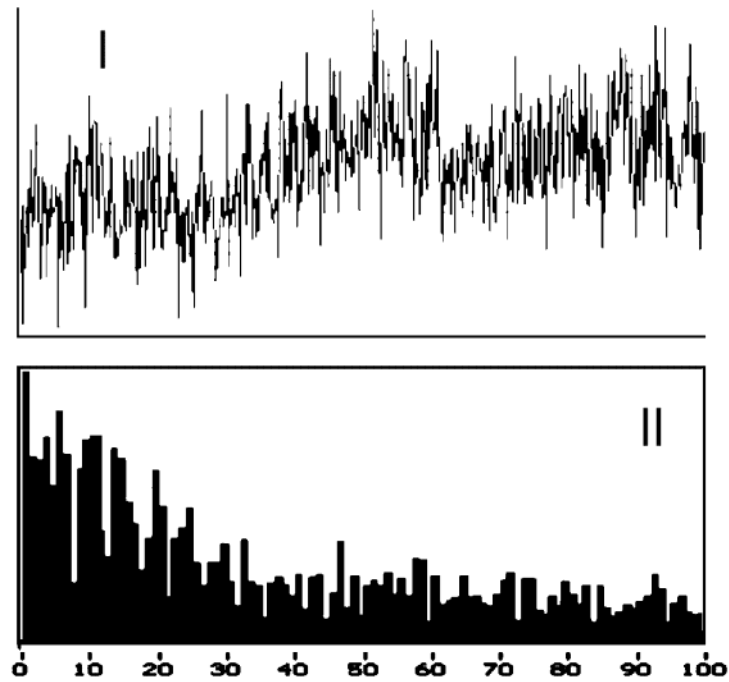


Figure 9 The average grey density distribution along three sections parallel to central axis of DR image of anoxic sediments core (I) and corresponding FFT (II)

For this core, we have counted about 225 laminae whose thickness varied between 2 and 4 mm. By supposing that these are annual laminae, we have measured the variation of corresponding opacity of the DR image, finally obtaining a typical graph reproduced in Figure 9. After we have performed a three point smoothing, a power spectrum of fast Fourier transform of resulting time series presented a relative maximum in the region of low frequencies, corresponding to a periodicity of about 7 years (Figure 9). Such procedure of direct investigation of sedimentation cycles starting from CAT or DR similar to those reported in ref. [42] could be very useful in every preliminary analysis of any long term sedimentary processes or paleoclimatic reconstruction.

4. Concluding Remarks

A single anode potential-double set of X-ray detector home made dual-energy computer tomograph have been used to investigate a number of samples consisting of diverse organic as well as inorganic materials such as fluor and sulfur containing polymers, domestic goods that on a normal radiography generate the same signature such as soap, paper, leather, tooth past, the content of spray tubes, etc. as well as fragments of metamorphic rocks or unconsolidated sediment cores.

By using a filtered back projection reconstruction algorithm and a set of standard samples with well known densities and effective atomic numbers it was possible to reconstruct the distribution function of densities and effective atomic numbers in any transverse section of investigated objects with a maximum precision of 3.5 % and respectively 2 %.

In the case of metamorphic rocks different details such as hidden planes, internal fractures, well developed garnets or fractions having different granulation have been evidenced in all DECAT images. Moreover, from density and effective atomic number histograms it was possible to calculate the halfwidth of these functions, values in concordance with the mineralogical composition of investigated samples.

In the case of unconsolidated sediments cores, the most representative results were obtained by means of digital radiography performed by using the same dual-energy computer tomograph, helping us to evidence a great variety of lithofacies such as cross bedded sediments, ripple cross laminations, planar cross bedded sand horizontally bedded sand showing a parallel lamination, or depositions zone with an appreciable concentration of heavy minerals, all of them reflecting the local conditions of transport and deposition. Moreover, the Black Sea core collected 600 m below sea surface showed about 225 distinct laminae, 2 to 4 mm thick that by means of time series analysis revealed a periodicity of about 7 years.

All these results recommend noninvasive dual-energy computer axial tomography and digital radiography as very versatile methods for investigation, appropriate for a great diversity of organic as well as mineral samples.

5. Acknowledgment

This work was supported by the Romanian Ministry for Education and Research (grants CNCSIS 293/2003, MENER 625/2005 and ROSA 1R/1/2005).

6. References

- [1] Hounsfield, G.N. (1973) Computerised transverse axial scanning (tomography) Part 1: Description of system, *British Journal of Radiology*, 46, 1016-1022,
- [2] Ackerman, J.L., Ellingson, W.A. (1991) *Advanced Tomographic Imaging Methods for the Analysis of Materials*, Materials Research Society, Pittsburgh, 218pp.
- [3] Reimers, P., Goebels, J., Weise, H.-P., Wilding, K. (1984) Some aspects of industrial non-destructive evaluation by X- and γ -ray computed tomography. *Nuclear Instruments and Methods in Physics Research* 221, 201–206.
- [4] Toye, D., Crine, M., Marchot, M. (2005) Imaging of liquid distribution in reactive distillation packings with a new high energy x-ray tomograph, *Measurements Science and Technology* 16, 2213-20.
- [5] Hirakimoto, A. (2001) Microfocus X-ray computed tomography and its industrial applications, *Analytical Sciences* 17 (suppl.) I123-I125.
- [6] Jacobs, P., Sevens, E., Kunnen, M. (1995) Principles of computerized X-ray tomography and applications to building materials. *The Science of Total Environment*, 167, 161-170.
- [7] Hunt, P., Engler, P., Bajsarowicz, C. (1988) Computed tomography as a core analysis tool: applications, instrument evaluation and image improvement techniques. *Journal of Petroleum Technology* 40, 1203-1210.
- [8] Dului, O.G. (1999) Computer Axial Tomography in geosciences: an overview, *Earth-Science Review*, 48, 265 – 281
- [9] Ketcham, R.A., Carlson, W.D. (2001) Acquisition, optimization and interpretation of X-ray computed tomographic imagery: applications to the geosciences, *Computers & Geosciences* 27, 381-400.
- [10] Rodríguez-Rey, A., Ruiz de Argandoña, V.G., Calleha, L., Suárez del Rio, L.M. (2004) X-ray tomography characterization of microfissuration on rocks generated by freeze-thaw cycles. In *X-ray for Geomaterials, Soils, Concrete, Rocks: Proceedings of the International Workshop on X-ray CT for Geomaterials-GEOX2003*, (J. Otani and Y. Obara Eds.), 6-7 November 2003, Kumamoto, Japan, Balkema, Lisse, pp. 293-298.
- [11] Seidler, G.T., Martinez, G., Seeley, L.H., Kim, K.H., Behne, E.A., Zaranek, S., Chapman, B.D. (2000) Heald, SM Brewes, DL. (2000) Granule-by-granule reconstruction of a sandpile from X-Ray microtomography data. *Physical Review E* 62, 8175-8181.
- [12] Trapp J, Bäck S Å J, Lepage M, Michael G and Baldock C 2001 An experimental study of the dose response of polymer gel dosimeters imaged with x-ray computed tomography *Physics in Medicine and Biology*. 46, 2939–51
- [13] Bosscher, H. (1993) Computerized tomography and skeletal density of coral skeleton. *Coral Reef* 12, 97-103.
- [14] Ekevad, M. (2004) Method to compute fiber directions in wood from computed tomography image, *Journal of Wood Science* 50, 41–46
- [15] Nickel, M., Beckmann, F. (2002) The 3-dimensional sponge skeleton: Synchrotron x-ray computed microtomography enables new insights into functional morphology. In: Krell U, Schneider JR, von Zimmermann M (Eds.) *HASYLAB Annual Report 2002. Part I*, 919-920. Print / CD-ROM / Online: http://www-hasylab.desy.de/science/annual_reports/2002_report/index.html

- [16] Rodiles-Hernández, R., Hendrickson, D.A., Lundberg, J.G., Humphries, J.M. (2005) *Lacantunia enigmatica* (Teleostei: Siluriformes) a new and phylogenetically puzzling freshwater fish from Mesoamerica, *Zootaxa* 1000, 1–24
- [17] Masschaele, B., Dierick, M., Cnudde, V., Van Hoorebeke, L., Delputte, S., Gildemeister, A., Gaehler, R., Hillenbach, A. (2004) High-speed thermal neutron tomography for the visualization of water repellents, consolidants and water uptake in sand and lime stones, *Radiation Physics and Chemistry* 71, 807–808
- [18] Winkler, B., Knorr, K., Kahle, A., Vontobel, P., Lehmann, E., Hennion, B., Bayon, G. (2002) Neutron imaging and neutron tomography as non-destructive tools to study bulk-rock samples. *European Journal of Mineralogy*, 14, 349-354.
- [19] Kak, A.C., Slaney, M. (1999) *Principles of Computerized Tomographic Imaging*, IEEE Press, New York.
- [20] Herman, G.T. (1980) *Image reconstruction from projections. The Fundamentals of Computerized Tomography*, Academic Press, New York.
- [21] Kalender, W.A. (2001) *Computed Tomography: Fundamentals, System Technology, Image Quality, Applications*, MCD, Munich.
- [22] Feldkamp, L. A., Davis, L.C., Kress, J. W. (1984) Practical cone-beam algorithm, *Journal of the Optical Society of America* 1, 612-619.
- [23] McCollough, C. H. (1999) Performance evaluation of a multi-slice CT system, *Medical Physics* 26, 2223-2230.
- [24] Landis, E.N., Nagy, E.N., Keane, D.T. (2003) Microstructure and fracture in three dimensions, *Engineering Fracture Mechanics* 70, 911–925
- [25] Fuchs, T., Kachelriess, M., Kalender, W.A. (2000) Technical advances in multi-slice spiral CT, *European Journal of Radiology*. 36, 69–73.
- [26] Natterer, F. (1986) *The Mathematics of Computerized Tomography*, J. Wiley & Sons, New York.
- [27] Brooks, R.A., Di Chiro, G. (1976) Principles of computed assisted tomography CAT in radiography and radioisotopic imaging. *Physics in Medicine and Biology* 21, 689–752.
- [28] Censor, Y., Gordon, D., Gordon, R. (2001) Component averaging: an efficient iterative parallel algorithm for large and sparse unstructured problems, *Parallel Computing* 27, 777-808.
- [28] Iovea, M., Vamvakoussis, A., Mateiasi, G., Georgiou, V., Samoilis G., Neagu, M. (2001) Development of digital radiography control and industrial tomography for non-destructive testing in Greece. *The British Institute of Non-Destructive Testing, Insight*, 43, 362-368
- [29] Hunt, P., Engler, P., Bajsarowicz, C., (1988) Computed tomography as a core analysis tool: applications, instrument evaluation and image improvement techniques. *Journal of Petroleum Technology* 40, 1203-1210.
- [30] Rizescu, C., Besliu, C., Jipa, A. (2001): Determination of local density and effective atomic number by the dual-energy computerized tomography method with the ¹⁹²Ir radioisotope, *Nuclear Instruments and Methods in Physics Research A*. 465, 584-599.
- [31] Siegbahn, K. (1968): *Alpha, beta and gamma ray spectroscopy*, North Holland, Amsterdam.
- [32] Aylmore, L.A.G. (1993) Use of computer assisted tomography in studying water movement around plant roots. *Advances in Agronomy*, 49, 1-54.
- [33] Rogasik, H., Crawford, J. W., Wendroth, O., Young I.M., Joschko, M., Ritz, K. (1999) Discrimination of soil phases by dual energy X-ray tomography. *Soil Science Society of America Journal* 63, 741-751.
- [34] Braz, D., Lopes. R.T., Motta, L.G.M. (200) Dual-energy computerized tomography in compacted soil, *Geotechnical and Geological Engineering* 18, 221-238.
- [35] Van Geet, M., Swennen, Wevers, M. (2001) Towards 3-D petrography.: application of microfocus computer tomography in geological science. *Computers & Geosciences* 27, 1091-1099.
- [36] Dului, O.G., Rizescu, C.T. Ricman, C. (2003) Dual energy gamma-ray axial computer tomography investigation of some metamorphic and sedimentary rocks, *Neues Jahrbuch für Geologie und Paläontologie* 228, 343-362.
- [37] Iovea, M., Oaie, G., Ricman, C., Mateiasi, G., Neagu, M., Szobotka, S., Dului, O.G. (2005), Dual energy X-ray computer axial tomography and digital radiography investigation of cores and other objects of geological interest, submitted to *Engineering Geology*.
- [38] Algeo T.J., Phillips M., Jaminski J., Fenwieck M. (1994), High Resolution X- radiography of Laminated Sediment Cores, *Journal of Sedimentary Research* A64, 665 – 668.
- [39] Iovea, M., Oaie, G., Dului, O.G., Neagu, M., Mateiasi, G. (2006) Digital radiography and X-ray computer tomography investigations of unconsolidated geological samples (Danube River, Danube Delta and Black Sea sediments), *Geophysical Research Abstracts*, 8, abstract # 03165.
- [40] Miall, A.D. (1996) *The geology of fluvial deposits, sedimentary facies, basin analysis and petroleum geology*, Springer Verlag, Heidelberg.
- [41] Manoleli, D., Nalbant, T. (1976) *Black Sea life*, Scientific and Encyclopedic Press, Bucharest (in Romanian).
- [42] Boespflug, X., Long, B., Occhietti, S. (1995) Cat-scan in marine stratigraphy: a quantitative approach. *Marine Geology* 122, 281– 301.